Supplementary information

Atomic Layer Deposition of Cobalt Using H_2-, N_2- and NH_3-based Plasmas: On the Role of the Co-reactant

Martijn F. J. Vos[1], Gerben van Straaten[1], W.M.M. (Erwin) Kessels[1] and Adriaan J.M. Mackus[1,]*

[1]Department of Applied Physics, Eindhoven University of Technology, P.O. Box 513, 5600 MB Eindhoven, The Netherlands

*E-mail: a.j.m.mackus@tue.nl

Metals and metal nitrides deposited using NH_3 and H_2/N_2 plasmas

Table S1. List of selected metals and metal nitrides which have been deposited using NH_3 plasma and/or H_2/N_2 plasma as co-reactant. The third column indicates whether the use of NH_3 and/or H_2/N_2 plasma resulted in a metal or metal nitride film. In addition the reduction potential E^0 of the corresponding element is listed.[2] As the reduction potential decreases, C, O, and N incorporation (and therefore metal nitride deposition) become more likely. In general, the use of a NH_3 or H_2/N_2 plasma yields metal deposition for reduction potentials of ~ -0.3 and above, while for elements below Co a metal nitride film is obtained. Note that W and Mo do not follow the trend based on the reduction potential. W and Mo are however reported to be very prone to nitridation and their nitrides are stable.[1]

Element	Reported co-reactant(s)	Reported state	Reference	E^0 (eV)
Pt	NH_3	metal	3	1.180
Ir	NH_3	metal	4	1.156
Pd	H_2/N_2	metal	5	0.951
Ag	NH_3	metal	6	0.800
Ru	NH_3 & H_2/N_2	metal	7,8	0.455
Ni	NH_3	metal	9	-0.257
Co	NH_3 & H_2/N_2	metal	10–12	-0.280
W	NH_3 & H_2/N_2	nitride	13	0.100
Mo	H_2/N_2	nitride	14	-0.200
In	H_2/N_2	nitride	15	-0.338
Ga	NH_3 & H_2/N_2	nitride	15,16	-0.549
Ta	NH_3 & H_2/N_2	nitride	17–19	-0.600
Nb	NH_3 & H_2/N_2	nitride	20,21	-1.100
Ti	NH_3 & H_2/N_2	nitride	22,23	-1.163
Hf	H_2/N_2	nitride	24	-1.550
Al	NH_3 & H_2/N_2	nitride	16,25	-1.662

ALD behavior

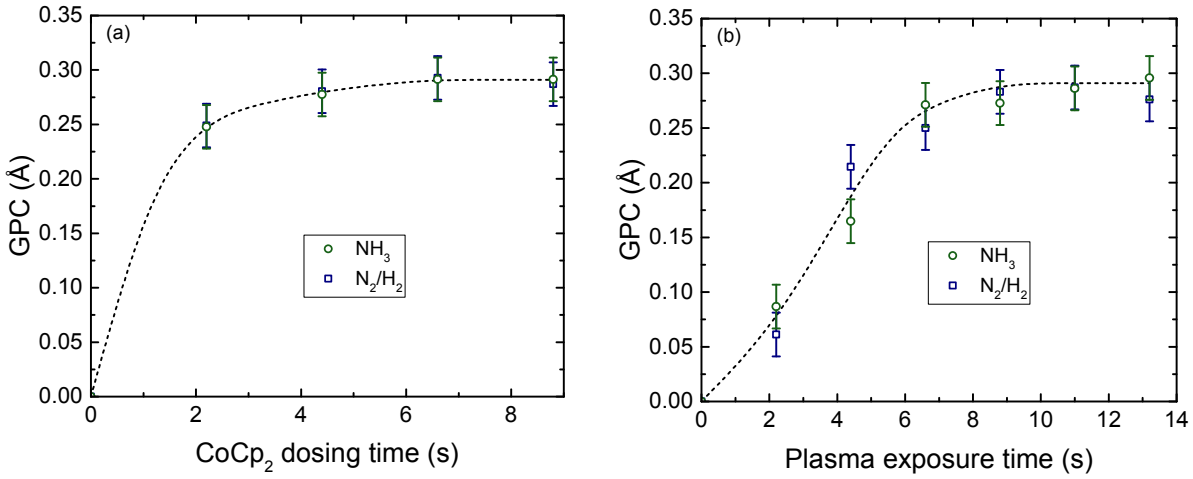

Figure S1. Growth per cycle (GPC) as a function of (a) $CoCp_2$ dosing time and (b) plasma exposure time for the AB-NH_3- and the AB-H_2/N_2 processes, plotted in the same graphs. The default $CoCp_2$ dosing time and plasma exposure time were 6 s and 10 s, respectively. The lines serve as guides to the eye. The saturation curves for the two processes look very similar and the GPC in saturation is approximately the same (0.29 ± 0.02 Å). The precursor dosing time shows saturation after roughly 5 s, and a plasma exposure time of 9 s is needed to reach saturation.

Procedure for time-resolved quadrupole mass spectrometry measurements

To be able to differentiate between signals caused by reaction products from signals caused by species present due to either the precursor dosing, source gasses, or plasma ignition, different types of cycles were used. These three different cycles were: a 'normal' ALD cycle, a cycle without precursor dosing and a cycle without igniting the plasma(s). See Figure S2 for schematics of the three different cycles.

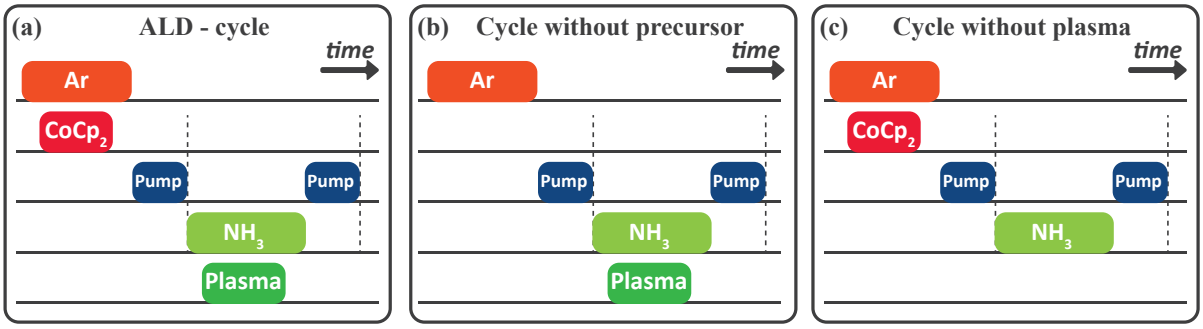

Figure S2. Schematic illustrations showing the three different cycles that were used for the QMS studies for the case of the AB-NH_3 process.

The three different sets of cycles were performed sequentially. Fig. S3 shows an example of the raw data that is collected by this procedure. As can be seen, every set of ten ALD cycles was preceded by plasma cleaning steps or a 'plasma reset'. This plasma reset consisted of a 90 s O_2 plasma (to remove contamination from the reactor wall), a reducing NH_3 plasma for 120 s, and a final pump step of 60 s. For each set of ten cycles, the signal over the last nine was averaged, since the first cycle was typically affected by the plasma reset.

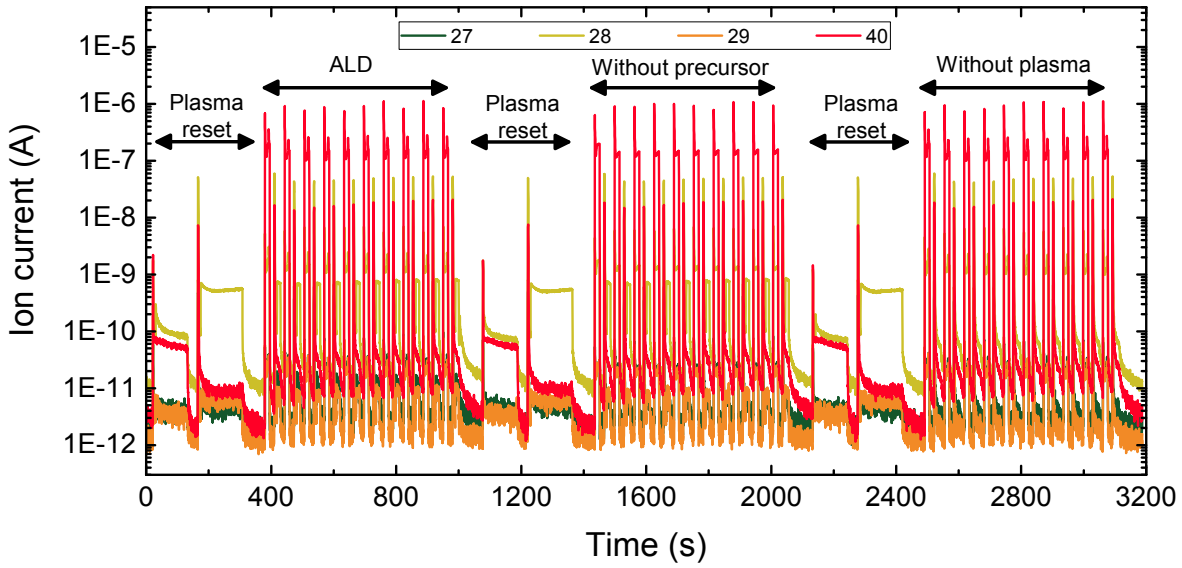

Figure S3. Raw QMS data collected for four different *m/z* ratios (27, 28, 29 and 40, see legend). Three different sets of cycles were performed, separated from each other by plasma resets.

Assignment of species to *m/z* ratios

Table S2. *m/z* ratios, their assigned ions and their (main) assigned parent molecules. The assignments are based on cracking patterns taken from the NIST database.

m/z	Assigned ion(s)	Assigned parent species	*m/z*	Assigned ion(s)	Assigned parent species
2	H_2^+	H_2	27	$C_2H_3^+$, HCN^+	C_2H_4, C_5H_6, HCN
12	C^+	HCN	28	N_2^+, $C_2H_4^+$	N_2, C_2H_4
13	CH^+	HCN	39	$C_3H_3^+$, C_2HN^+	C_5H_6, C_3H_4, $Co(C_5H_5)_2$, C_2HN
14	N^+	N_2, NH_3	40	Ar^+, $C_3H_4^+$, $C_2H_2N^+$	Ar, C_3H_4, C_5H_6, C_2H_2N
15	NH^+	NH_3	59	Co^+	$Co(C_5H_5)_2$
16	NH_2^+	NH_3	65	$C_5H_5^+$	C_5H_6, $Co(C_5H_5)_2$
17	NH_3^+	NH_3	66	$C_5H_6^+$	C_5H_6, $Co(C_5H_5)_2$
18	H_2O^+, NH_4^+	H_2O, NH_3	98	$CoC_3H_3^+$	$Co(C_5H_5)_2$
24	C_2^+	C_2H_4, C_5H_6	124	$Co(C_5H_5)^+$	$Co(C_5H_5)_2$
25	C_2H^+	C_2H_4, C_5H_6	189	$Co(C_5H_5)_2^+$	$Co(C_5H_5)_2$
26	$C_2H_2^+$, CN^+	C_2H_4, C_5H_6, HCN			

Comparison NH_3 and H_2/N_2 plasma

QMS spectra

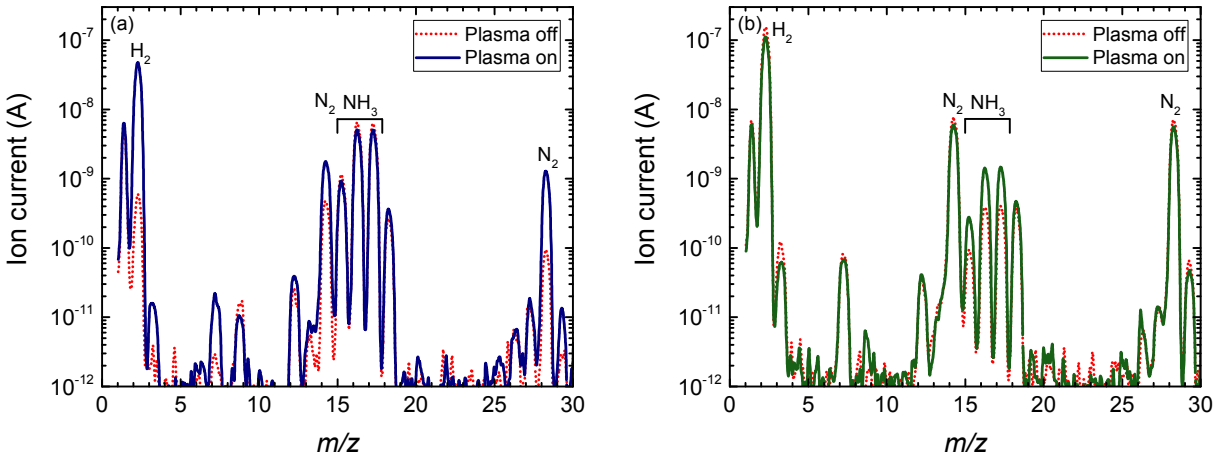

Figure S4. QMS mass spectra for (a) NH_3 and (b) H_2/N_2, gas and plasma. The spectra were collected for the source gas only ('plasma off', dashed line) and after plasma ignition ('plasma on', solid line). Comparison of the two spectra in (a) indicates that part of the NH_3 is dissociated upon plasma ignition, leading to formation of N_2 (m/z = 14 and 28) and H_2 (m/z = 1 and 2). On the contrary, (b) shows that part of the H_2 and N_2 in the H_2/N_2 plasma is consumed, leading to the formation of NH_3, as revealed by the increase in ion current for m/z ratios 15-17.

OES spectra

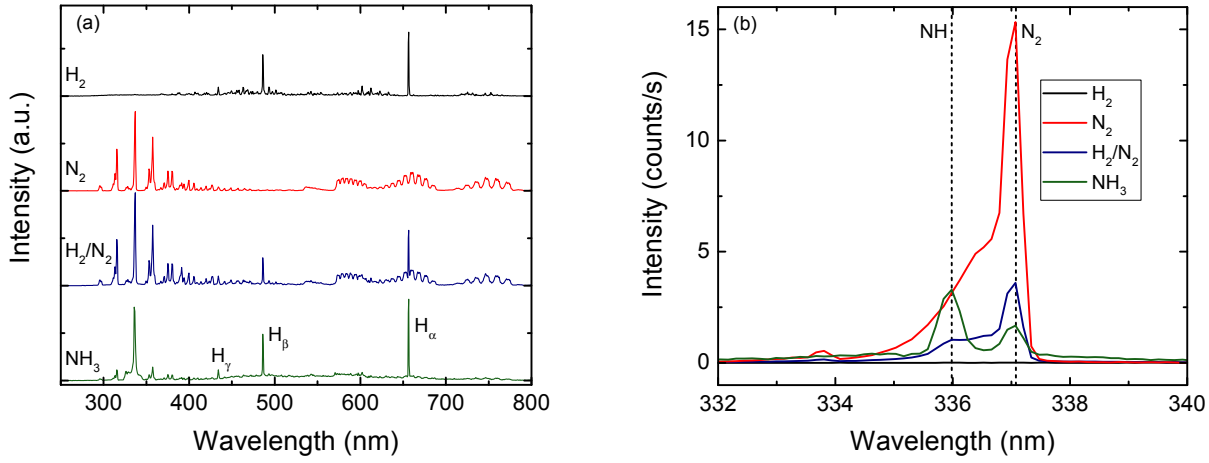

Figure S5. Optical emission spectra for H_2, N_2, H_2/N_2 and NH_3 plasmas over the wavelength range of (a) 280 nm – 800 nm and (b) 332 nm – 340 nm. The emission spectra for the NH_3 and H_2/N_2 plasmas are very similar. (a) The spectra have been scaled and offset for clarity. (b) An emission line for excited NH can be seen at ~336 nm in the spectra for both plasmas, indicating that $NH_{x,\,x<3}$ radical species are present.

QMS precursor half-cycle

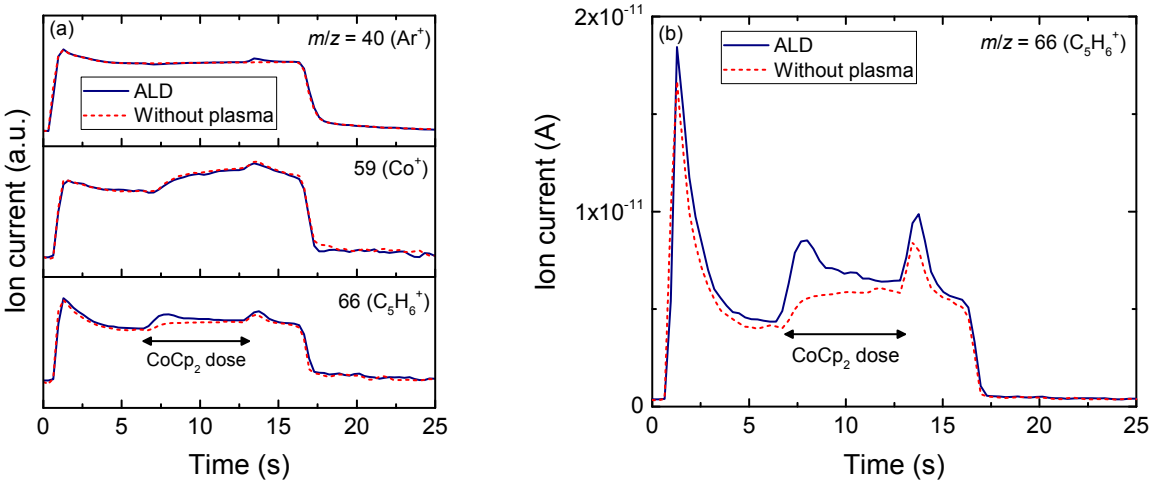

Figure S6. (a) Time-resolved QMS signals for *m/z* ratios 40 (Ar^+), 59 (Co^+) and 66 ($C_5H_6^+$), collected during the precursor sub-cycle of the AB-NH_3 process, plotted on a logarithmic vertical scale. (b) The QMS signal for *m/z* =66, plotted using a linear vertical scale. QMS measurements were done for the normal ALD cycle, and for a reference cycle without igniting the plasma, both using a $CoCp_2$ dose of 6 s. Comparing the two signals gives insight into which species are formed as a consequence of the ALD reactions. Note that the Ar carrier gas is diverted before sending it through the $CoCp_2$ bubbler in order to stabilize the gas flow. This leads to an increase in chamber pressure, which explains the initial increase in ion currents just after t = 0. After the Ar starts flowing through the bubbler at around 7 s (indicated with an arrow in the figure), the ion currents for *m/z* ratios 59 and 66 increase, related to Co^+ and HCp^+ ($C_5H_6^+$), respectively. Subsequently changing the Ar gas flow from the bubbler to the purge line at t = 13 s leads to a pressure spike, accompanied by a peak in the ion currents. During the 'normal' ALD cycle the increase at t = 7s for *m/z* = 66 is significantly higher than for the reference cycle without plasma exposure (note that the vertical scale is logarithmic in (a)). This difference in ion current suggests that HCp is released when the precursor molecule chemisorbs to the surface. Note that similar QMS measurements for the AB-H_2/N_2 process also revealed the release of HCp during precursor dosing, suggesting a similar reaction mechanism.

QMS cracking patterns

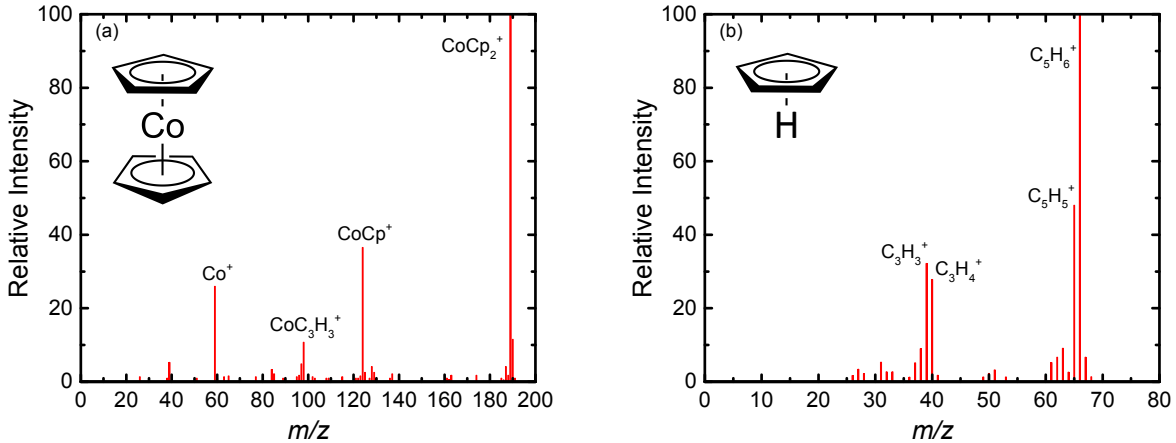

Figure S7. QMS cracking patterns for (a) $CoCp_2$ and (b) HCp, both taken from the NIST database. The cracking pattern for $CoCp_2$ is dominated by signals at *m/z* = 59 (Co), 124 (CoCp) and 189 ($CoCp_2$). Signals at 39, 40, 65 and 66 are the main contributions in case of HCp.

X-ray photoelectron spectroscopy

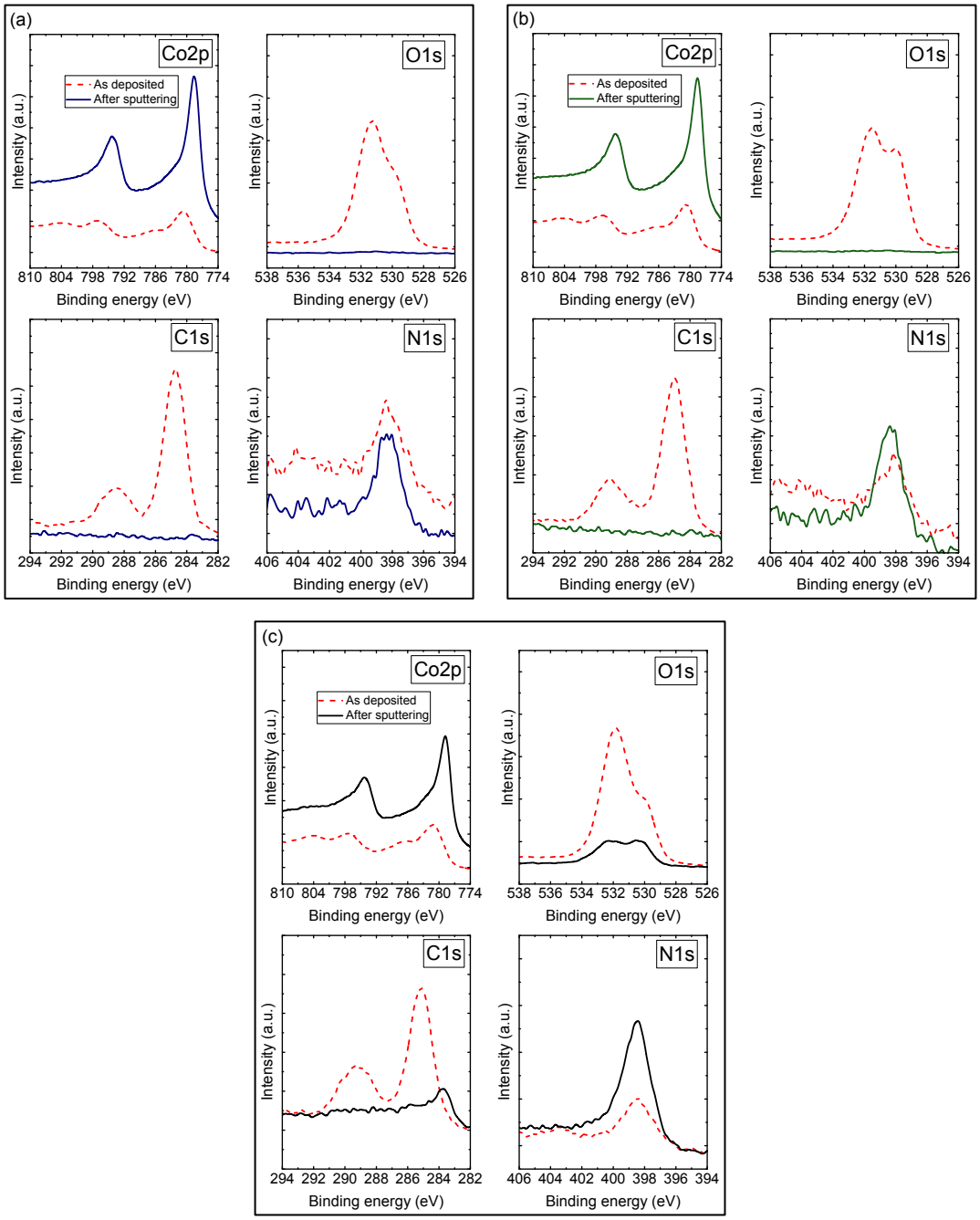

Figure S8. XPS spectra for the Co2p, O1s, C1s and N1s peaks for Co films deposited using the (a) AB-NH_3 process, (b) the AB-H_2/N_2 process and (c) the ABC-N_2-H_2 process. 1000 cycles were performed for all samples. 6 minutes Ar^+ sputtering was applied to remove the surface contamination. The films deposited using the AB-NH_3- and AB-H_2/N_2 processes contain small amounts of impurities, while the film deposited using the ABC-N_2-H_2 process is significantly contaminated with O, C and N. The surface of the films is slightly oxidized. However, the metallic Co2p peaks is visible around 780.2 eV after Ar^+ sputtering, for the films deposited using the AB-processes.

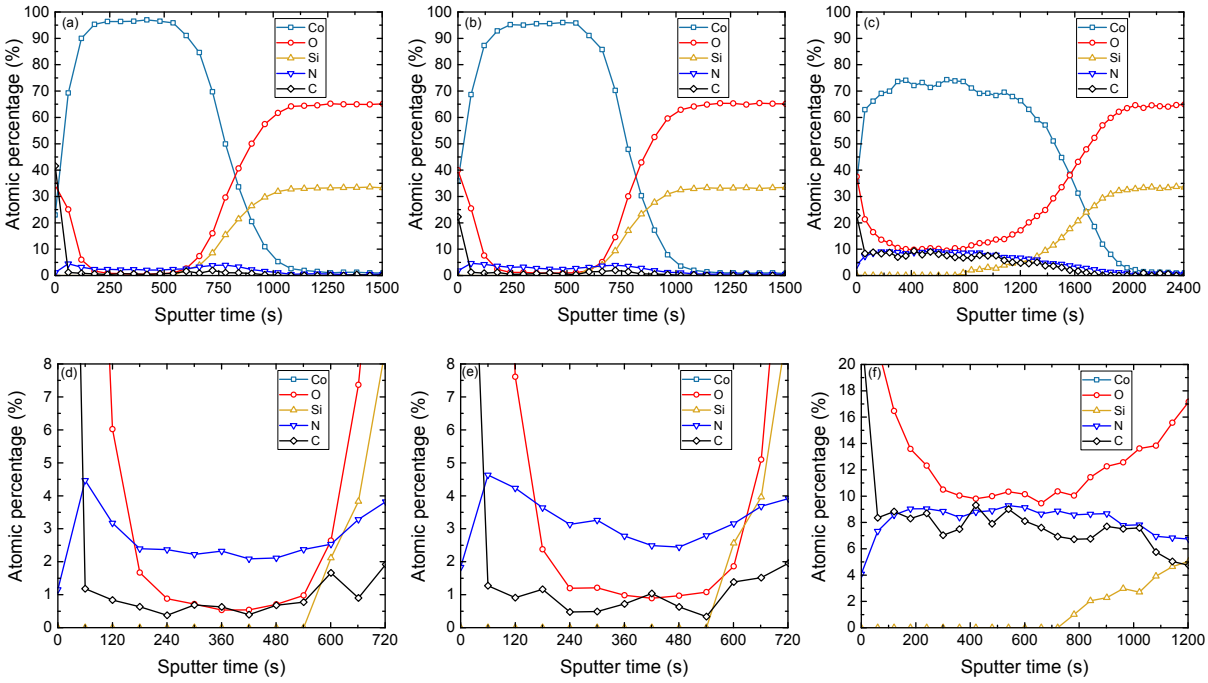

Figure S9. XPS depth profiles for Co films deposited using (a, d) the AB-NH_3 process, (b, e) the AB-H_2/N_2 process and (c, f) the ABC-N_2-H_2 process. 1000 cycles were performed for all samples. (e - f) show the impurity contents (O, N and C) in more detail. For the AB-NH_3 process and the AB-H_2/N_2 process the N-content is slightly higher in the subsurface region (~4.5 at.% as compared to ~2.5 at.%), suggesting that N species (e.g. NH_y) are more stable on the surface than in the bulk. Moreover, the trend of the N-content corroborates the out diffusion of N.

Table S3. Material properties of Co films for the ABC-processes as determined from SE, four-point probe and XPS. Two different three-step processes were used, an ABC-cycle with the N_2 plasma first, followed by the H_2 plasma and an ABC-cycle with the H_2 plasma first followed by the N_2 plasma. The impurity contents were determined using XPS after sputtering with Ar^+ for 6 min.

ALD Process	Cycles	d (nm)	ρ (μΩ·cm)	[O] (at.%)	[N] (at.%)	[C] (at.%)
ABC – N_2 – H_2	1000	44	$1x10^3$	10.1	8.4	7.2
ABC – H_2 – N_2	350	28	$7x10^3$	8.9	8.5	7.8

Ion current as a function of H_2/N_2 mixing ratio

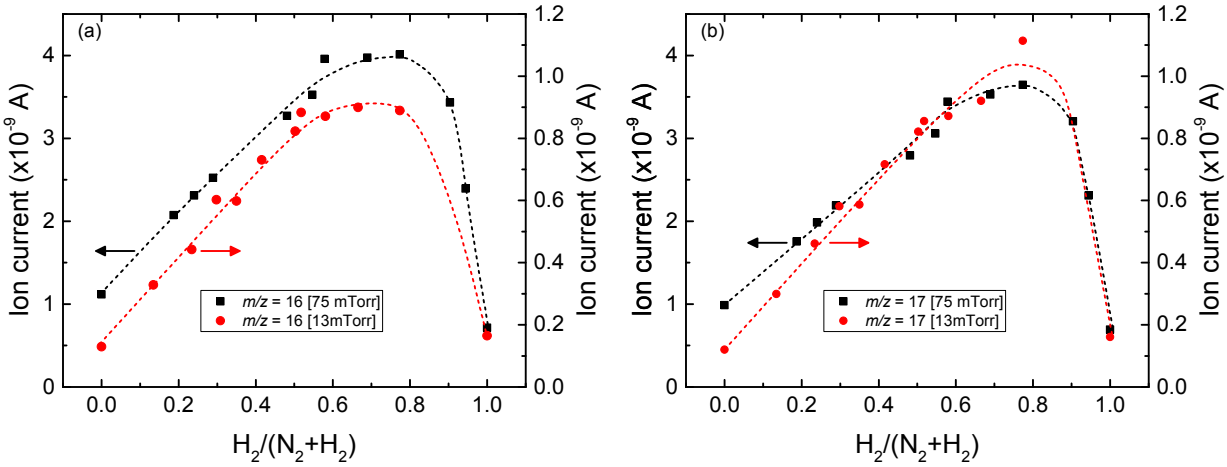

Figure S10. QMS ion current at (a) *m/z* ratio 16 and (b) *m/z* ratio 17 as a function of H_2 fraction in the H_2/N_2 gas mixture, for a pressure of 13 mTorr and 75 mTorr. The ion currents at *m/z* ratios 16 and 17 are measures for the NH_3 content in the H_2/N_2 plasma. The lines are guides to the eye. Due to the low gas flows used for a pressure of 13 mTorr, it is not possible to keep the pressure constant for mixing ratios higher than ~80 Vol.%. As mentioned in the main text, adding N_2 gas to the H_2 gas increases the pumping speed, thereby changing the total pressure. This makes obtaining certain mixing ratios for a constant total pressure not straightforward. However, the similarities between the trends for the two different pressures confirm that the optimum in the NH_3 production corresponds to 70 Vol.% - 80 Vol.% H_2, both at 13 mTorr and 75 mTorr. The data for 75 mTorr is also shown in the main text in Figure 3.

References

(1) Wang, T.; Yan, Z.; Michel, C.; Pera-Titus, M.; Sautet, P. Trends and Control in the Nitridation of Transition-Metal Surfaces. *ACS Catal.* **2018**, *8*, 63–68.

(2) Rumble, J. R. *CRC Handbook of Chemistry and Physics*, 98th Editi.; CRC-Press: Boca Raton, FL, 2017.

(3) Longrie, D.; Devloo-Casier, K.; Deduytsche, D.; Van den Berghe, S.; Driesen, K.; Detavernier, C. Plasma-Enhanced ALD of Platinum with O2, N2 and NH3 Plasmas. *Ecs J. Solid State Sci. Technol.* **2012**, *1*, Q123–Q129.

(4) Kim, S.-W.; Kwon, S.-H.; Jeong, S.-J.; Park, J.-S.; Kang, S.-W. Improvement of Morphological Stability of PEALD-Iridium Thin Films by Adopting Two-Step Annealing Process. *Electrochem. Solid-State Lett.* **2008**, *11*, H303.

(5) Ten Eyck, G. A.; Pimanpang, S.; Juneja, J. S.; Bakhru, H.; Lu, T. M.; Wang, G. C. Plasma-Enhanced Atomic Layer Deposition of Palladium on a Polymer Substrate. *Chem. Vap. Depos.* **2007**, *13*, 307–311.

(6) Minjauw, M. M.; Solano, E.; Sree, S. P.; Asapu, R.; Van Daele, M.; Ramachandran, R. K.; Heremans, G.; Verbruggen, S. W.; Lenaerts, S.; Martens, J. A.; et al. Plasma-Enhanced Atomic Layer Deposition of Silver Using Ag(Fod)(PEt3) and NH3-Plasma. *Chem. Mater.* **2017**, *29*, 7114–7121.

(7) Xie, Q.; Jiang, Y. L.; Musschoot, J.; Deduytsche, D.; Detavernier, C.; Van Meirhaeghe, R. L.; Van den Berghe, S.; Ru, G. P.; Li, B. Z.; Qu, X. P. Ru Thin Film Grown on TaN by Plasma Enhanced Atomic Layer Deposition. *Thin Solid Films* **2009**, *517*, 4689–4693.

(8) Hong, T. E.; Mun, K.; Choi, S.; Park, J.; Kim, S.-H.; Cheon, T.; Kim, W. K.; Lim, B.; Kim, S. Atomic Layer Deposition of Ru Thin Film Using N2/H2 Plasma as a Reactant. *Thin Solid Films* **2012**, *520*, 6100–6105.

(9) Lee, H. B. R.; Bang, S. H.; Kim, W. H.; Gu, G. H.; Lee, Y. K.; Chung, T. M.; Kim, C. G.; Park, C. G.; Kim, H. Plasma-Enhanced Atomic Layer Deposition of Ni. *Jpn. J. Appl. Phys.* **2010**, *49*.

(10) Lee, H.-B.-R.; Kim, H. High-Quality Cobalt Thin Films by Plasma-Enhanced Atomic Layer Deposition. *Electrochem. Solid-State Lett.* **2006**, *9*, G323.

(11) Yoon, J.; Lee, H.-B.-R.; Kim, D.; Cheon, T.; Kim, S.-H.; Kim, H. Atomic Layer Deposition of Co Using N2/H2 Plasma as a Reactant. *J. Electrochem. Soc.* **2011**, *158*, H1179.

(12) Park, J.; Lee, H. B. R.; Kim, D.; Yoon, J.; Lansalot, C.; Gatineau, J.; Chevrel, H.; Kim, H. Plasma-Enhanced Atomic Layer Deposition of Co Using Co(MeCp)2 Precursor. *J. Energ. Chem.* **2013**, *22*, 403–407.

(13) Sowa, M. J.; Yemane, Y.; Prinz, F. B.; Provine, J. Plasma-Enhanced Atomic Layer Deposition of Tungsten Nitride. *J. Vac. Sci. Technol. A Vacuum, Surfaces, Film.* **2016**, *34*, 051516.

(14) Bertuch, A.; Keller, B. D.; Ferralis, N.; Grossman, J. C.; Sundaram, G. Plasma Enhanced Atomic Layer Deposition of Molybdenum Carbide and Nitride with Bis(*Tert* -Butylimido)Bis(Dimethylamido) Molybdenum. *J. Vac. Sci. Technol. A Vacuum, Surfaces, Film.* **2017**, *35*, 01B141.

(15) Alevli, M.; Gungor, N. Influence of N2/H2 and N2 Plasma on Binary III-Nitride Films Prepared by Hollow-Cathode Plasma-Assisted Atomic Layer Deposition. *J. Vac. Sci. Technol. A Vacuum, Surfaces, Film.* **2018**, *36*, 01A110.

(16) Ozgit-Akgun, C.; Goldenberg, E.; Okyay, A. K.; Biyikli, N. Hollow Cathode Plasma-Assisted Atomic Layer Deposition of Crystalline AlN, GaN and AlxGa1−xN Thin Films at Low Temperatures. *J. Mater. Chem. C* **2014**, *2*, 2123–2136.

(17) Kim, H.; Kellock, A. J.; Rossnagel, S. M. Growth of Cubic-TaN Thin Films by Plasma-Enhanced Atomic Layer Deposition. *J. Appl. Phys.* **2002**, *92*, 7080–7085.

(18) Kim, H.; Detavenier, C.; Van Der Straten, O.; Rossnagel, S. M.; Kellock, A. J.; Park, D. G. Robust TaNx Diffusion Barrier for Cu-Interconnect Technology with Subnanometer Thickness by Metal-Organic Plasma-Enhanced Atomic Layer Deposition. *J. Appl. Phys.* **2005**, *98*, 014308.

(19) Han, J. H.; Kim, H. Y.; Lee, S. C.; Kim, D. H.; Park, B. K.; Park, J. S.; Jeon, D. J.; Chung, T. M.; Kim, C. G. Growth of Tantalum Nitride Film as a Cu Diffusion Barrier by Plasma-Enhanced Atomic Layer Deposition from Bis((2-(Dimethylamino)Ethyl)(Methyl)Amido)Methyl(Tert-Butylimido)Tantalum Complex. *Appl. Surf. Sci.* **2016**, *362*, 176–181.

(20) Huotari, H.; Haukka, S.; Matero, R.; Rahtu, A.; Tois, E.; Tuominen, M. Atomic Layer Deposition of NbN and Nb(Si)N for Metal Electrodes. In *ECS Transactions*; ECS, 2006; Vol. 1, pp 131–135.

(21) Sowa, M. J.; Yemane, Y.; Zhang, J.; Palmstrom, J. C.; Ju, L.; Strandwitz, N. C.; Prinz, F. B.; Provine, J. Plasma-Enhanced Atomic Layer Deposition of Superconducting Niobium Nitride. *J. Vac. Sci. Technol. A Vacuum, Surfaces, Film.* **2017**, *35*, 01B143.

(22) Kim, J. Y.; Seo, S.; Kim, D. Y.; Jeon, H.; Kim, Y. Remote Plasma Enhanced Atomic Layer Deposition of TiN Thin Films Using Metalorganic Precursor. *J. Vac. Sci. Technol. A Vacuum, Surfaces, Film.* **2004**, *22*, 8–12.

(23) Kim, J. Y.; Kim, D. Y.; Park, H. O.; Jeon, H. Characteristics and Compositional Variation of TiN Films Deposited by Remote PEALD on Contact Holes. *J. Electrochem. Soc.* **2005**, *152*, G29.

(24) Kim, E.-J.; Kim, D.-H. Highly Conductive HfNx Films Prepared by Plasma-Assisted Atomic Layer Deposition. *Electrochem. Solid-State Lett.* **2006**, *9*, C123.

(25) Alevli, M.; Ozgit, C.; Donmez, I.; Biyikli, N. The Influence of N2/H2 and Ammonia N Source Materials on Optical and Structural Properties of AlN Films Grown by Plasma Enhanced Atomic Layer Deposition. *J. Cryst. Growth* **2011**, *335*, 51–57.